International Journal of Minerals, Metallurgy and Materials
Volume 28, Number 4, April 2021, Page 657
https://doi.org/10.1007/s12613-020-2097-x

Comprehensive analysis of pulsed plasma nitriding preconditions on the fatigue behavior of AISI 304 austenitic stainless steel

Okan Unal[1,2], *Erfan Maleki*[3], *and Remzi Varol*[4]

1) Mechanical Engineering Department, Karabuk University, Karabuk 78050, Turkey
2) Modern Surface Engineering Laboratory (MSELAB), Karabuk University, Karabuk 78050, Turkey
3) Mechanical Engineering Department, Sharif University of Technology-International Campus, Kish Island 79417-76655, Iran
4) Mechanical Engineering Department, Suleyman Demirel University, Isparta 32200, Turkey
(Received: 26 December 2019; revised: 30 March 2020; accepted: 11 May 2020)

Abstract: This study aims to draw an exact boundary for microstructural and mechanical behaviors in terms of pulsed plasma nitriding conditions. The pulsed plasma nitriding treatment was applied to AISI 304 austenitic stainless steel at different temperatures and durations. Results reveal that nitriding depth increased as process temperature and duration increase. The nitriding depth remarkably increased at 475°C for 8 h and at 550°C for 4 h. An austenite structure was transformed into a metastable nitrogen-oversaturated body-centered tetragonal expanded austenite (S-phase) during low-temperature plasma nitriding. The S-phase was converted to CrN precipitation at 475°C for 8 h and at 550°C for 4 h. Surface hardness and fatigue limit increased through plasma nitriding regardless of process conditions. The best surface hardness and fatigue limit were obtained at 550°C for 4 h because of the occurrence of CrN precipitation.

Keywords: pulsed plasma nitriding; S-phase; fatigue; nitrided layer

1. Introduction

AISI 304 austenitic stainless steel has been selected in many applications because of its effective corrosion resistance, nonmagnetic property, and biocompatible performance. However, it has poor hardness, strength, and wear that should be improved [1–3]. As such, mechanical surface treatments (e.g., surface mechanical attrition treatment [4], shot peening [5–8], and ultrasonic nanocrystal surface modification [9]) and thermal surface treatments [10–11] (e.g., carburizing [12] and plasma nitriding [11,13–15]) have been performed to increase hardness and wear resistance.

Nitriding processes should be applied to create thick nitride layers and achieve a remarkable wear–fatigue resistance performance. This performance is attributed to the characteristics of a nitrided zone. Nitrided layer thickness varies depending on process type, operating temperature and duration, and chamber environment. However, high processing temperature and long duration cause distortion in metal parts, and this outcome is often undesirable. Plasma nitriding is performed under high-density plasma with low vacuum pressure; therefore, temperature and duration can be reduced without sacrificing the performance of nitrided surfaces [16]. This treatment has been improved through the effect of glow discharge in terms of voltage and current adjustments. Glow discharge provides ionization, and ions have been bombarded to surfaces via a high voltage difference [17–19]. Exposing plasma energy to thermally treated surfaces improves outcomes within a short time and at low temperature by accelerating diffusion; thus, a controllable microstructure is formed [20–23]. Zhao *et al*. [24] focused on enhanced plasma-assisted nitriding operations, such as plasma ion implantation, plasma immersion ion implantation, and thermo-ionically assisted triode. These treatments have been applied to industrialized parts regardless of shape and dimension [25].

Plasma nitriding has been widely selected to improve the surface of austenitic stainless steel. The industrial requirement for these steels is their corrosion feature. However, the performance of wear and fatigue resistance must be within a reasonable range. Therefore, various studies on different surface treatments have been conducted. Plasma (ion) nitriding is a thermo-mechanical operation and applied at a range of 350–550°C. Nitrogen atoms diffuse through the acceleration of plasma energy in a shorter time compared with that of conventional counterparts [26–27]. This process creates a body-centered tetragonal expanded austenite (S-phase) and con-

Corresponding author: Okan Unal E-mail: unalokan78@gmail.com

sequently increases the surface hardness of austenitic stainless steels to HV 1000 [28–30].

For steels, an austenitic structure is prone to transformation into a metastable supersaturated nitrogen-rich S-phase at >450°C. The S-phase contributes high hardness and wear resistance performance. On the contrary, CrN precipitation begins to occur via the reduction of the Cr percentage in the matrix and leads to a remarkable loss of corrosion resistance performance [24]. Díaz-Guillén *et al*. [31] demonstrated the simultaneous combination of the S-phase and a chromium-nitrided structure via pulsed plasma nitriding within the range of 510–550°C. Lu *et al.* [32] showed that nitriding efficiency is low at 450°C. S-phase development with a high nitriding efficiency without degrading the corrosion resistance performance seems the main advantage of the treatment. Therefore, studies have focused on the rapid production of the S-phase [32].

This study aims to investigate the plasma nitriding preconditions in terms of phase alteration and transformation. Surface compound layer analysis, diffusion, and chemical changes were conducted to examine the fatigue–hardness performance. The previous literature results show that the treatment influences the S-phase, and the diffusion layer directly affects the microstructure and mechanical performance (wear, corrosion, and fatigue). Besides, various factors, such as frequency, gas mixture, furnace, process type (e.g., pulsed and active screen), and cycle, are considered for microstructural and mechanical alterations [18,23,30,33–35].

2. Experimental

AISI 304 austenitic stainless steel specimens were manufactured with cold drawn bars after quenching and annealing at 1050°C. The specification, chemical composition, and mechanical properties of steel specimens are shown in the Table 1.

Table 1. Specification, chemical composition, and mechanical properties of AISI 304 steel specimens

Specification								
Dimension / nm	Shape	Tolerance	Length / m			Piece	Weight / kg	
10000	Round	h9	3.0–3.2			566	1064	
Chemical composition / wt%								
C	Mn	Si	P	Cr	Ni	Cu	Mo	Co
0.04	1.68	0.4	0.03	18.24	8.0	0.6	0.26	0.17
Mechanical properties								
R_e (0.2%) / MPa	R_m / MPa	A / %	Z / %	Hardness (BHN)				
341	748	39	70	261				

Note: R_e (0.2%)—Yield strength; R_m—Tensile strength; A—Total elongation; Z—Reduction in area.

The as-received and plasma-nitrided specimens with a diameter of ϕ25 mm and a thickness of 5 mm for microstructural characterizations are shown in Fig. 1. Rotating bending fatigue specimens were manufactured in accordance with the DIN 50113 standard.

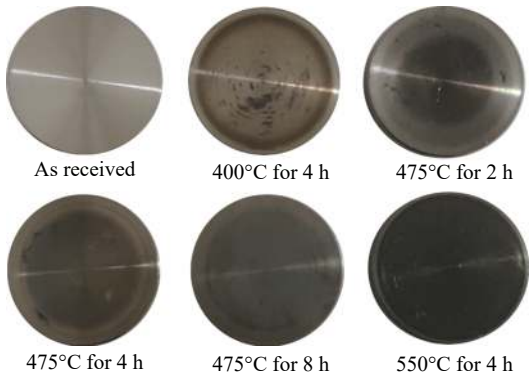

Fig. 1. As-received and the plasma-nitrided with different conditions specimens for microstructural characterization analysis.

Plasma nitriding was performed in a PLC-controlled pulsed plasma nitriding furnace. A gas mixture composed of 25vol% N_2 and 75vol% H_2 was fed to the environment, and the ratio was chosen on the basis of the effectivity of 15vol%–30vol% of N_2 [30,36–37]. The gas mixture was then fed to a chamber at approximately 500 Pa under the potential of 500 V. The pressure within the range of 100–130 Pa was accepted [38]. Accordingly, 500 V and 333 Pa of potential and vacuum pressure, respectively, were selected for the novel approaches [31,39]. When the conditions of chambers were common for all nitriding processes, minimum preliminary parameters were determined on the basis of previously described approaches on the detection of the influence of nitriding temperature and duration on microstructural and mechanical performance. The effect of each parameter was determined by independently keeping the temperature and duration constant. The plasma nitriding conditions of the specimens are shown in Table 2.

All the specimens were cut from cross-sections and grounded from 120-grade emery papers to 1200-grade emery

Table 2. Plasma nitriding conditions for specimens

Temperature / °C	Duration / h	Gas volume ratio / %
400	4	25 N_2–75 H_2
475	2	25 N_2–75 H_2
475	4	25 N_2–75 H_2
475	8	25 N_2–75 H_2
550	4	25 N_2–75 H_2

papers and polished with 3, 1, and 0.25 μm diamond paste. Thereafter, the specimens were etched with a solution containing 100 mL of water, 100 mL of hydrochloric acid, and 10 mL of nitric acid for 180–210 s. The specimens were analyzed through optical microscopy (OM) and scanning electron microscopy (SEM) with Nikon Eclipse MA100 and Carl Zeiss Gemini Sigma, respectively. They were also examined through X-ray diffraction (XRD) by using a Rigaku Smart Lab diffractometer with Cu K_α radiation (scanning speed, 2°/min; voltage, 40 kV; scanning angle, 20°–90°; current, 30 mA). Micro-hardness tests were performed by using a Qness GmbH Q10 tester with a load of 0.005 N and a duration of 10 s. Fatigue tests were conducted with a BESMAK BMT-250 rotating bending fatigue tester by applying a frequency of 50 Hz and a constant stress amplitude of $R = -1$. Load was manually controlled with a load cell, and tests were performed via the DOLI software.

3. Results and discussion

3.1. Characterization of the nitrided layer

The OM observations of the nitrided specimens are shown in Fig. 2. The nitrided layer can be distinguished via OM because of a strict boundary line between the core and the surface-treated layer. In general, the nitriding depth increases as process duration and temperature increase. The minimum nitriding depth is obtained at 400°C for 4 h, and microstructural alterations can be detected on the outmost layer. The thickness of the nitrided layers is similar at 475°C with the durations of 2 and 4 h. The nitriding depth remarkably increased at 475°C for 8 h and at 550°C for 4 h. The color of the layer also darkens under these conditions. Dark (black) precipitations begin to emerge at 475°C for 8 h, and the layer completely becomes black at 550°C for 4 h (Fig. 2).

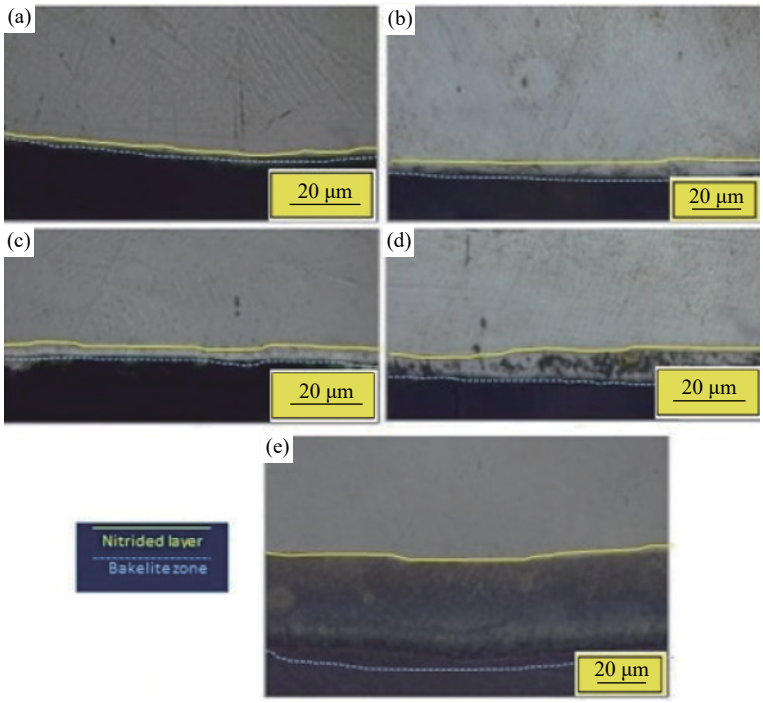

Fig. 2. OM observations of plasma-nitrided specimens with different conditions: (a) 400°C for 4 h; (b) 475°C for 2 h; (c) 475°C for 4 h; (d) 475°C for 8 h; (e) 550°C for 4 h.

The SEM observations (Fig. 3) show that the nitrided layer was compatible with the OM. The nitrided layer thickness of the specimens treated at 475°C for 2 and 4 h seems similar under OM; however, the distinction was observed clearly through SEM analysis. Detailed analysis reveals the formation of dark precipitate at 475°C for 8 h, and the dark precipitate covers the whole nitrided layer at 550°C for 4 h. Energy dispersive X-ray (EDX) and XRD analyses supports the finding that chromium increases at 475°C for 8 h and at 550°C for 4 h (Figs. 4–5). Feugeas *et al.* [40] demonstrated that S-phase gradually and substantially transforms to CrN and Fe–N compounds through the application of plasma nitrid-

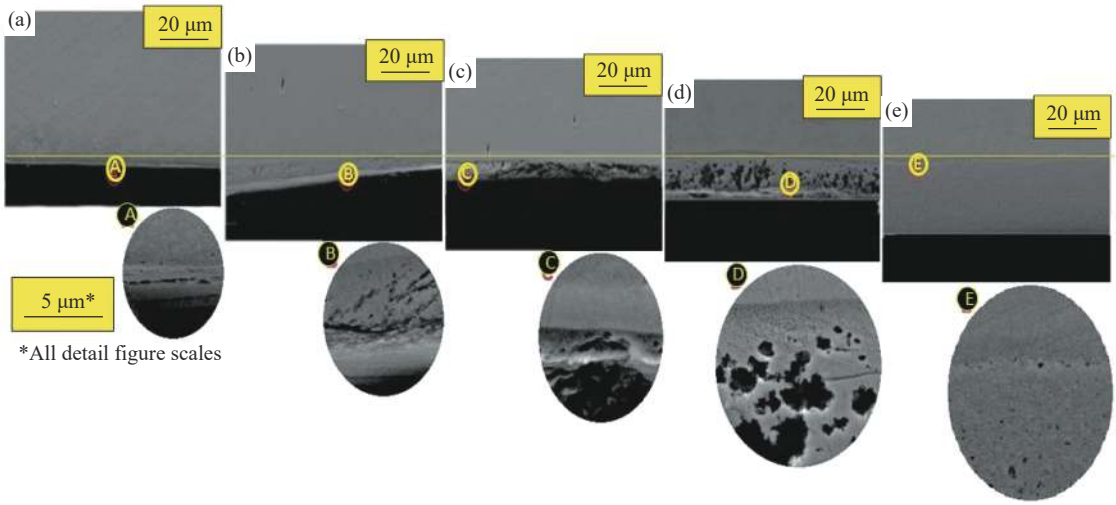

Fig. 3. SEM observations of plasma-nitrided specimens with different conditions: (a) 400°C for 4 h; (b) 475°C for 2 h; (c) 475°C for 4 h; (d) 475°C for 8 h; (e) 550°C for 4 h.

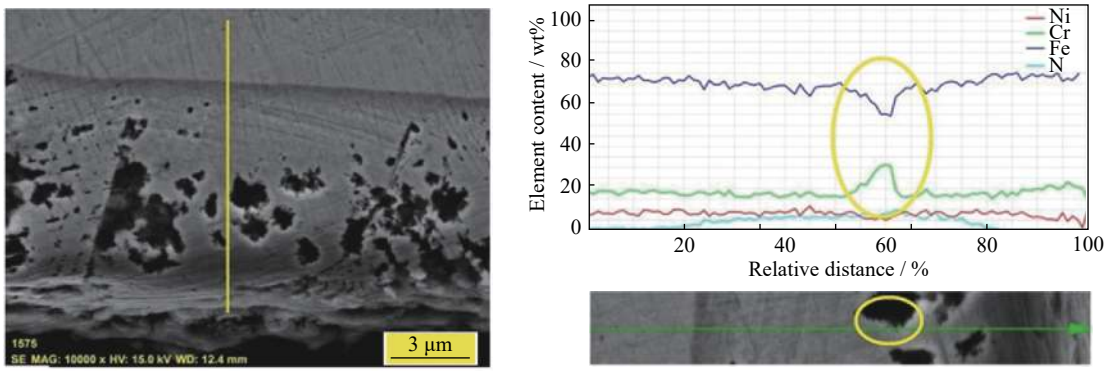

Fig. 4. EDX elemental analysis of nitride layers at 475°C for 8 h.

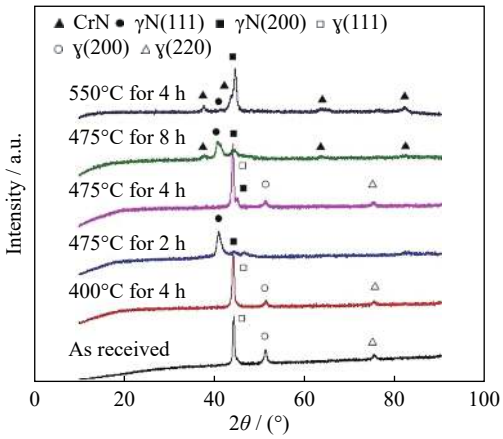

Fig. 5. X-ray diffraction peaks of the as-received and nitrided specimens.

ing at high temperatures and long durations. Liang *et al.* [41] claimed that the S-phase may reach its maximum saturation level at 420°C.

Shen *et al.*[1] stated that CrN forms on the nitrided layer at high temperatures, and Cr particles migrate from the grain interior to the boundaries. Shen *et al.* [29] applied plasma nitriding to AISI 304 in the range of 410–520°C for 4 h and changed vacuum pressure and potential within 410–420 Pa and 600–650 V, respectively. They achieved substantial CrN precipitation at 520°C. The duration was not adequate for CrN precipitation at 480°C, and SEM investigations and XRD results show that no precipitation occurs on the S-phase. The compound layer thickness observed at 410 and 480°C was consistent with that at 400 and 475°C for the same duration. Balusamy *et al.* [42] demonstrated the plasma nitriding of AISI 304 with direct current (DC) application at 500 V/2.67 Pa (potential/pressure) via 20%/80% N_2/H_2 volume ratio at 500°C for 8 h. Despite the high temperature and long duration, the compound layer was 4 μm. This result is attributed not only to processing temperature and duration but also to chamber potential, vacuum pressure, gas feeding performance, and other important treatment parameters.

XRD analysis (Fig. 5) reveals austenite peaks at different 2θ of the as-received specimens. Although a very thin influenced layer different from the core was observed at OM and SEM observations at 400°C for 4 h (Figs. 2(a) and 3(a)), no

crystallographic alterations were detected in XRD analysis. Austenite transforms into an oversaturated nitride S-phase (γ_N) through plasma nitriding [43–44]. The conversion of austenite peaks to the S-phase exerts compressive residual stress on the nitrided layer [39]. Nitriding begins at 475°C for 2 h, and the S-phase and γ(111) peaks were observed. The S-phase was detected via low-temperature plasma nitriding, and its mechanical properties can be increased without losing the corrosion resistance performance. However, increasing the nitriding temperature and duration causes the conversion of S-phase to Fe_4N and CrN. Under different plasma nitriding conditions, CrN, Fe_4N, and $Fe_{2-3}N$ forms [45]. Xia *et al*. [46] clarified the decomposition of S-phase and the occurrence of new chemical reactions of elements with nitrogen. Balusamy *et al.* [42] presented CrN precipitation at 500°C for 8 h and conducted XRD analysis; however, they could not observe precipitations through microstructural investigations. In some cases, the order of transformation can be changed. In the plasma nitriding of austenitic stainless steel (AISI 303), austenite is chemically converted to the S-phase, and the S-phase is transformed to ferrite and CrN precipitations. Solubility capacity increases as the operating temperature increases [47]. Thus, the decomposition of the S-phase leads to the formation of ferrite and CrN phases as revealed by the broadened ferrite peak and the raised CrN peak. Gontijo *et al.*[48] observed that nitriding at 500°C subsequently results in conversion to Fe_4N, Fe_2N, and α ferrite phases.

The changes in the microhardness of the nitrided specimens are presented in Fig. 6. The surface hardness reaches HV 1200 at 475°C for 8 h and at 550°C for 4 h. However, surface hardness can be increased up to HV 700 only when the temperature is 475°C and the durations are 2 and 4 h. Surface hardness remainsat HV 500 at 400°C for 4 h. Hardness improves because of the precipitation of CrN and the existence of γ_N phases [24]. CrN forms because of the excessive solution of nitrogen through the S-phase at high temperatures and long durations. CrN and Fe–N become stable and enhance hardness because of the S-phase [45]. The intensification of the compounds on XRD analysis is applied to surface hardness at 475°C for 8 h and at 550°C for 4 h.

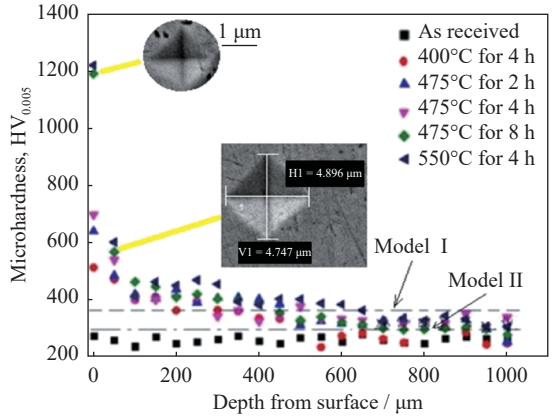

Fig. 6. Change in the hardness of the as-received and nitrided specimens from the surface to the core. The SEM figures demonstrate the indentation trace shown by yellow lines.

The indentations on the nitrided zone are shown in Fig. 7. The interior indentation diagonals are two to three times longer than the surface indentation trace. Diffusion occurs from the surface to the interior during plasma nitriding. The nitrogen concentration profile abruptly decreases through the interior, and the effectivity of the S-phase, CrN, and Fe–N compound percentages gradually decreases. As such, the maximum level of hardness (the minimum diagonal trace) is accomplished on the outmost layer.

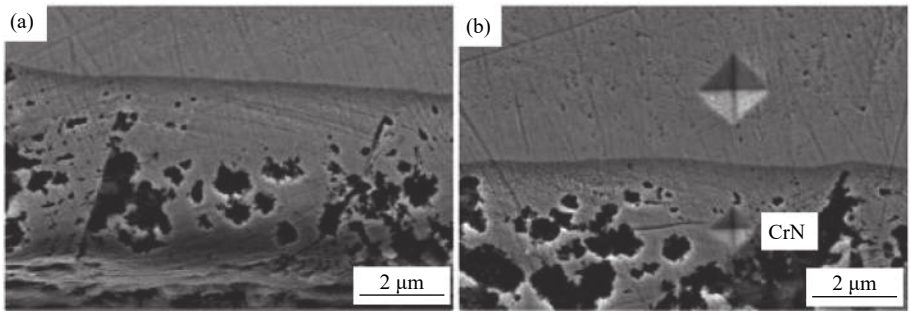

Fig. 7. SEM images of the nitrided specimen at 475°C for 8 h: (a) nitride layer; (b) indentation trace.

Two approaches are generally applied to determine the depth of a nitrided layer. In Model I, a boundary line was constructed by adding HV 100 to the core hardness; in Model II, a boundary line was created by increasing the hardness of 10% [49–50]. The nitrided and influenced depths based on the models were shown in Table 3.

3.2. Fatigue resistance

The stress amplitude–number of cycle (S–N) curves of all the treated specimens are shown in Fig. 8. At a certain stress amplitude, the S–N curve of iron-based alloys flattens, and they can be assessed to have an infinite life. The fatigue limit of the as-received AISI 304 is 215 MPa. The limit increases

Table 3. Nitrided layer thickness based on models I and II

Plasma nitriding conditions	Nitrided layer thickness / μm	Influenced depth / μm	
		Model I	Model II
400°C for 4 h	—	300	500
475°C for 2 h	3–4	450	950
475°C for 4 h	4–5	250	1000
475°C for 8 h	7–8	450	950
550°C for 4 h	30–32	650	1000

to 260 MPa after nitriding at 400°C for 4 h. However, the layer is too thin to be measured at 400°C for 4 h. XRD analysis also revealed no transformation or occurrence on the nitriding layer. Conversely, hardness and fatigue limit slight increases. The reason for these changes can be expressed in terms of the high-temperature regime with nitrogen on the surface. For heating–cooling routes, the surface can be modified with a hard deposition. The fatigue limit increases to 355 and 600 MPa at 475°C for 2 h and at 550°C for 4 h, respectively. The endurance limits are close to each other at 475°C for 8 h and at 550°C for 4 h. Although the nitrided zone thicknesses are similar at 475°C for different durations, the effective fatigue resistance is enhanced during the treatment for 8 h. Hardness improvement and potential compressive residual stress application are the dominant mechanisms, not nitrided layer thickening. Moreover, the fatigue limit at 550°C for 4 h is the highest among the treatments because the diffusion layer thickens and hardens. It also retards crack occurrence and propagation because of the complete substantial transformation of the S-phase to a CrN/Fe–N compound layer, which is more stable and harder. Riazi *et al*. [51] demonstrated that plasma nitriding duration is more effective than temperature although compound layer saresix times thick. The results showed that the influence of preconditions (nitriding chamber and time–temperature conditions) should be concentrated and detected in terms of microstructural and mechanical behaviors.

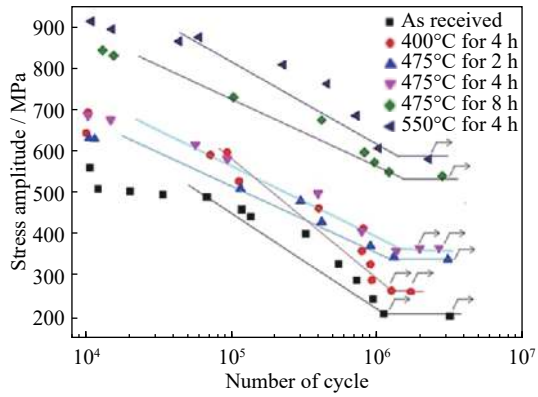

Fig. 8. S–N curves of the as-received and plasma nitrided specimens.

Fig. 9 reveals the fatigue fracture surface of the as-received and treated specimens. In the as-received specimens, failure occurs through the formation of multi crack initiation sites supported by inner micro-cracks. At short nitriding dur-

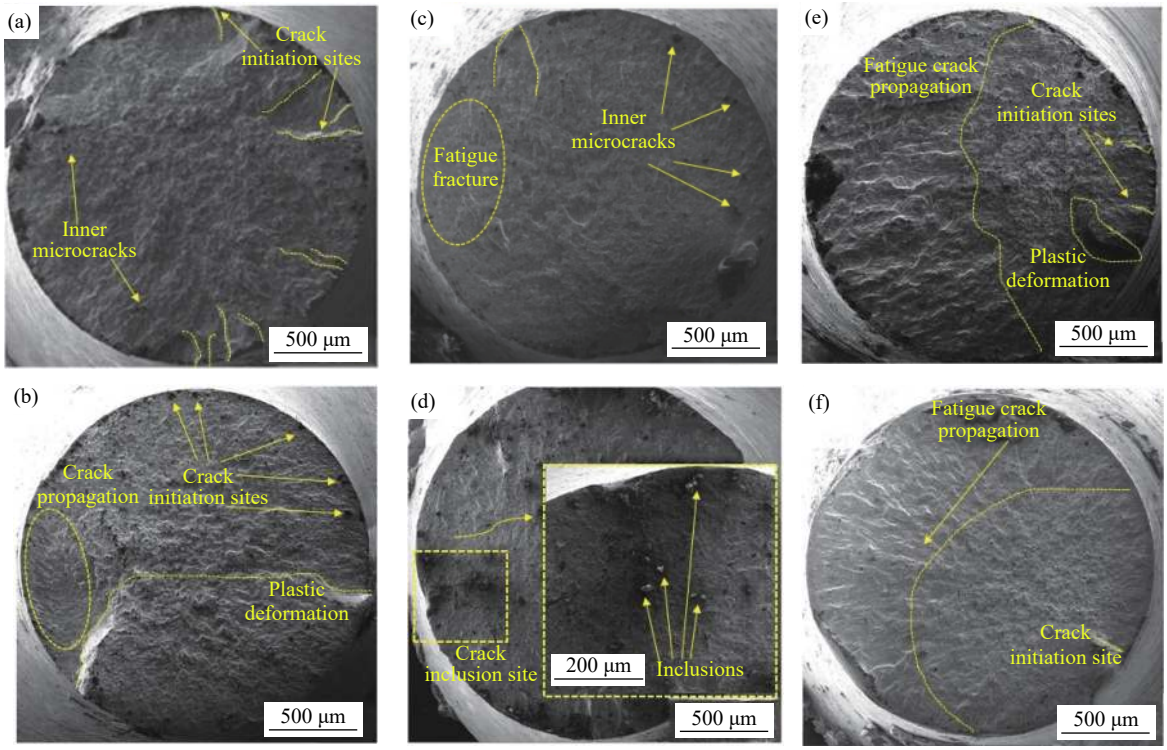

Fig. 9. SEM observations of the fractured surface of different specimens: (a) as received; (b) nitrided at 400°C for 4 h; (c) nitrided at 475°C for 2 h; (d) nitrided at 475°C for 4 h; (e) nitrided at 475°C for 8 h; (f) nitrided at 550°C for 4 h.

ations, surface compression by residual stress and hard zone diminish the surface crack initiation zone, and subsurface inner micro-cracks has the dominant effect on the fracture (Fig. 9(c)). Inclusions are also one of the crucial mechanisms of fatigue fracture shown in Fig. 9(f). Inclusions create stress concentrations, so they behave as initial micro-crack formation points. Similarly, Wu *et al*. [52] proposed two fundamental approaches for fatigue fracture behaviors. In one of the approaches, a surface crack initiated and caused a fracture. In the other approach, a subsurface crack initially formed because of the prevention of a nitrided layer and various inclusion types, such as Al_2O_3, CaO, and other oxides, which were located on the subsurface.

4. Conclusions

(1) Nitriding depth increased as process duration and temperature increase. The minimum nitriding depth was obtained at 400°C for 4 h. The nitriding depth remarkably increased at 475°C for 8 h and at 550°C for 4 h.

(2) An S-phase was observed when low-temperature plasma nitriding was applied and the hardness of the zone was increased. The S-phase was substantially converted to CrN precipitation at 475°C for 8 h and at 550°C for 4 h.

(3) The effective hardness on the surface improved under two nitride conditions (475°C for 8 h and 550°C for 4 h). The deepest nitrided zone was obtained at 550°C for 4 h.

(4) Plasma nitriding achieved surface hardness and increased fatigue limit regardless of process conditions; nevertheless, the best hardness and fatigue limit was obtained because of CrN precipitation.

(5) Fatigue fracture was observed in multi crack initiation sites in the as-received specimen. For the nitrided specimens, subsurface inner micro cracks and inclusions became the dominant effect on the fracture.

Acknowledgement

The authors would like to thank the Scientific and Technological Research Council of Turkey (TUBITAK) for the support of this study (Grant No: 215M134).

References

[1] Y.F. Shen, X.X. Li, X. Sun, Y.D. Wang, and L. Zuo, Twinning and martensite in a 304 austenitic stainless steel, *Mater. Sci. Eng. A*, 552(2012), p. 514.

[2] O. Unal and R. Varol, Surface severe plastic deformation of AISI 304 via conventional shot peening, severe shot peening and repeening, *Appl. Surf. Sci.*, 351(2015), p. 289.

[3] H.Y. Shen and L. Wang, Corrosion resistance and electrical conductivity of plasma nitrided titanium, *Int. J. Hydrogen Energy*, 46(2021), No. 19, p. 11084.

[4] S. Liu, S.Y. Gao, Y.F. Zhou, X.L. Xing, X.R. Hou, Y.L. Yang, and Q.X. Yang, A research on the microstructure evolution of austenite stainless steel by surface mechanical attrition treatment, *Mater. Sci. Eng. A*, 617(2014), p. 127.

[5] K. Zhan, C.H. Jiang, and V. Ji, Effect of prestress state on surface layer characteristic of S30432 austenitic stainless steel in shot peening process, *Mater. Des.*, 42(2012), p. 89.

[6] O. Unal, Optimization of shot peening parameters by response surface methodology, *Surf. Coat. Technol.*, 305(2016), p. 99.

[7] O. Unal and E. Maleki, Shot peening optimization with complex decision-making tool: Multi criteria decision-making, *Measurement*, 125(2018), p. 133.

[8] O. Unal, E. Maleki, I. Kocabas, H. Yilmaz, and F. Husem, Investigation of nanostructured surface layer of severe shot peened AISI 1045 steel via response surface methodology, *Measurement*, 148(2019), art. No. 106960.

[9] A. Amanov, R. Karimbaev, E. Maleki, O. Unal, Y.S. Pyun, and T. Amanov, Effect of combined shot peening and ultrasonic nanocrystal surface modification processes on the fatigue performance of AISI 304, *Surf. Coat. Technol.*, 358(2019), p. 695.

[10] O. Unal, E. Maleki, and R. Varol, Plasma nitriding of gradient structured AISI 304 at low temperature: Shot peening as a catalyst treatment, *Vacuum*, 164(2019), p. 194.

[11] O. Unal, E. Maleki, and R. Varol, Effect of severe shot peening and ultra-low temperature plasma nitriding on Ti–6Al–4V alloy, *Vacuum*, 150(2018), p. 69.

[12] L. Ceschini, C. Chiavari, E. Lanzoni, and C. Martini, Low-temperature carburised AISI 316L austenitic stainless steel: Wear and corrosion behaviour, *Mater. Des.*, 38(2012), p. 154.

[13] K.L. Ou, H.H. Chou, C.M. Liu, and P.W. Peng, Surface modification of austenitic stainless steel with plasma nitriding for biomedical applications, *Surf. Coat. Technol.*, 206(2011), No. 6, p. 1142.

[14] K.J. Lin, X.Y. Li, H.S. Dong, P. Guo, and D.D. Gu, Nitrogen mass transfer and surface layer formation during the active screen plasma nitriding of austenitic stainless steels, *Vacuum*, 148(2018), p. 224.

[15] Y.D. Zhu, J.W. Yao, M.F. Yan, Y.X. Zhang, Y.X. Wang, Y. Yang, and L. Yang, High temperature plasma nitriding to modify Ti coated C17200 Cu surface: Microstructure and tribological properties, *Vacuum*, 147(2018), p. 163.

[16] J. Schuster, E. Bruder, and C. Müller, Plasma nitriding of steels with severely plastic deformed surfaces, *J. Mater. Sci.*, 47(2012), No. 22, p. 7908.

[17] N. Kashaev, H.R. Stock, and P. Mayr, Nitriding of Ti–6%Al–4%V alloy in the plasma of an intensified glow discharge, *Met. Sci. Heat Treat.*, 46(2004), p. 294.

[18] K. Nikolov, K. Bunk, A. Jung, P. Kaestner, G. Bräuer, and C.P. Klages, High-efficient surface modification of thin austenitic stainless steel sheets applying short-time plasma nitriding by means of strip hollow cathode method for plasma thermochemical treatment, *Vacuum*, 110(2014), p. 106.

[19] L. Qin, L.H. Tian, A.L. Fan, B. Tang, and Z. Xu, Fatigue behavior of surface modified Ti–6Al–4V alloy by double glow discharge plasma alloying, *Surf. Coat. Technol*, 201(2007), No. 9-11, p. 5282.

[20] Z. Huang, Z.X. Guo, L. Liu, Y.Y. Guo, J. Chen, Z. Zhang, J.L. Li, Y. Li, Y.W. Zhou, and Y.S. Liang, Structure and corrosion behavior of ultra-thick nitrided layer produced by plasma nitriding of austenitic stainless steel, *Surf. Coat. Technol.*, 405(2021), art. No. 126689.

[21] S. Corujeira Gallo and H. Dong, On the fundamental mechanisms of active screen plasma nitriding, *Vacuum*, 84(2009), No. 2, p. 321.

[22] H. Aghajani, M. Torshizi, and M. Soltanieh, A new model for growth mechanism of nitride layers in plasma nitriding of AISI H11 hot work tool steel, *Vacuum*, 141(2017), p. 97.
[23] A. Yazdani, M. Soltanieh, and H. Aghajani, Active screen plasma nitriding of Al using an iron cage: Characterization and evaluation, *Vacuum*, 122(2015), p. 127.
[24] Y.H. Zhao, B.H. Yu, L.M. Dong, H. Du, and J.Q. Xiao, Low-pressure arc plasma-assisted nitriding of AISI 304 stainless steel, *Surf. Coat. Technol.*, 210(2012), p. 90.
[25] J. Morgiel and T. Wierzchoń, New estimate of phase sequence in diffusive layer formed on plasma nitrided Ti–6Al–4V alloy, *Surf. Coat. Technol.*, 259(2014), p. 473.
[26] R. Kertscher and S.F., Brunatto On the kinetics of nitride and diffusion layer growth in niobium plasma nitriding, *Surf. Coat. Technol.*, 401(2020), art. No. 126220.
[27] J. Fernández de Ara, E. Almandoz, J.F. Palacio, and G.G. Fuentes, Simultaneous ageing and plasma nitriding of grade 300 maraging steel: How working pressure determines the effective nitrogen diffusion into narrow cavities, *Surf. Coat. Technol.*, 317(2017), p. 64.
[28] T.T. Peng, Y. Chen, X.L. Liu, M.H. Wu, Y.Y. Lu, and J. Hu, Phase constitution control of plasma nitrided layer and its effect on wear behavior under different loads, *Surf. Coat. Technol.*, 403(2020), art. No. 126403.
[29] L. Shen, L. Wang, Y.Z. Wang, and C.H. Wang, Plasma nitriding of AISI 304 austenitic stainless steel with pre-shot peening, *Surf. Coat. Technol.*, 204(2010), No. 20, p. 3222.
[30] R. Valencia-Alvarado, A. de la Piedad-Beneitez, J. de la Rosa-Vázquez, R. López-Callejas, S.R. Barocio, O.G. Godoy-Cabrera, A. Mercado-Cabrera, R. Peña-Eguiluz, and A. E. Muñoz-Castro, Nitriding of AISI 304 stainless steel in a 85% H_2/15% N_2 mixture with an inductively coupled plasma source, *Vacuum*, 82(2008), No. 12, p. 1360.
[31] J.C. Díaz-Guillén, M. Naeem, J.L. Acevedo-Dávila, H.M. Hdz-García, J. Iqbal, M.A. Khan, and J. Mayen, Improved mechanical properties, wear and corrosion resistance of 316L steel by homogeneous chromium nitride layer synthesis using plasma nitriding, *J. Mater. Eng. Perform.*, 29(2020), No. 2, p. 877.
[32] S.J. Lu, X.B. Zhao, S.K. Wang, J.C. Li, W. Wei, and J. Hu, Performance enhancement by plasma nitriding at low gas pressure for 304 austenitic stainless steel, *Vacuum*, 145(2017), p. 334.
[33] R. Valencia-Alvarado, A. de la Piedad-Beneitez, J. de la Rosa-Vázquez, R. López-Callejas, S.R. Barocio, O.G. Godoy-Cabrera, A. Mercado-Cabrera, R. Peña-Eguiluz, and A. E. Muñoz-Castro, γ_N-shift as a function of N_2 content in AISI 304 nitriding, *Vacuum*, 81(2007), No. 11-12, p. 1434.
[34] K. Nikolov, K. Köster, P. Kaestner, G. Bräuer, and C.P. Klages, Strip hollow cathode method for plasma thermochemical treatment for surface modification of thin metal strips: Plasma nitriding of austenitic stainless steel sheets for bipolar plates, *Vacuum*, 102(2014), p. 31.
[35] A. de la Piedad-Beneitez, R. Valencia-Alvarado, R. López-Callejas, I. A. Rojas-Olmedo, R. Peña-Eguiluz, A. Mercado-Cabrera, S.R. Barocio, A.E. Muñoz-Castro, and B.G. Rodríguez-Méndez, Optimized AISI 304 steel nitriding in inductive RF N_2–H_2 plasmas, *Vacuum*, 85(2011), No. 12, p. 1149.
[36] J. Alphonsa, B.A. Padsala, B.J. Chauhan, G. Jhala, P.A. Rayjada, N. Chauhan, S.N. Soman, and P.M. Raole, Plasma nitriding on welded joints of AISI 304 stainless steel, *Surf. Coat. Technol.*, 228(2013), Suppl. 1, p. s306.
[37] S.K. Wang, W. Cai, J.C. Li, W. Wei, and J. Hu, A novel rapid D.C. plasma nitriding at low gas pressure for 304 austenitic stainless steel, *Mater. Lett.*, 105(2013), p. 47.
[38] J.C. Díaz-Guillén, G. Vargas-Gutiérrez, E.E. Granda-Gutiérrez, J.S. Zamarripa-Piña, S. I. Pérez-Aguilar, J. Candelas-Ramírez, and L. Álvarez-Contreras, Surface properties of Fe_4N compounds layer on aisi 4340 steel modified by pulsed plasma nitriding, *J. Mater. Sci. Technol.*, 29(2013), No. 3, p. 287.
[39] M. Asgari, A. Barnoush, R. Johnsen, and R. Hoel, Microstructural characterization of pulsed plasma nitrided 316L stainless steel, *Mater. Sci. Eng. A*, 529(2011), p. 425.
[40] J.N. Feugeas, B.J. Gomez, G. Sánchez, J. Ferron, and A. Craievich, Time evolution of Cr and N on AISI 304 steel surface during pulsed plasma ion nitriding, *Thin Solid Films*, 424(2003), No. 1, p. 130.
[41] W. Liang, Surface modification of AISI 304 austenitic stainless steel by plasma nitriding, *Appl. Surf. Sci.*, 211(2003), No. 1-4, p. 308.
[42] T. Balusamy, T.S.N. Sankara Narayanan, K. Ravichandran, I.S. Park, and M.H. Lee, Plasma nitriding of AISI 304 stainless steel: Role of surface mechanical attrition treatment, *Mater. Charact.*, 85(2013), p. 38.
[43] A. Galdikas and T. Moskalioviene, Modeling of stress induced nitrogen diffusion in nitrided stainless steel, *Surf. Coat. Technol.*, 205(2011), No. 12, p. 3742.
[44] T. Moskalioviene, A. Galdikas, J.P. Rivière, and L. Pichon, Modeling of nitrogen penetration in polycrystalline AISI 316L austenitic stainless steel during plasma nitriding, *Surf. Coat. Technol.*, 205(2011), No. 10, p. 3301.
[45] G.P. Singh, A. Joseph, P.M. Raole, P.K. Barhai, and S. Mukherjee, Phase formation in selected surface-roughened plasma-nitrided 304 austenite stainless steel, *Sci. Technol. Adv. Mater.*, 9(2008), No. 2, art. No. 025007.
[46] Y.Q. Xia, J.H. Hu, F. Zhou, Y.M. Lin, Y.L. Qiao, and T. Xu, Friction and wear behavior of plasma nitrided 1Cr18Ni9Ti austenitic stainless steel under lubrication condition, *Mater. Sci. Eng. A*, 402(2005), No. 1-2, p. 135.
[47] L.H. Lin, S.C. Chen, C.Z. Wu, J.M. Hung, and K.L. Ou, Microstructure and antibacterial properties of microwave plasma nitrided layers on biomedical stainless steels, *Appl. Surf. Sci.*, 257(2011), No. 17, p. 7375.
[48] L.C. Gontijo, R. Machado, E.J. Miola, L.C. Casteletti, N.G. Alcantara, and P.A.P. Nascente, Study of the S phase formed on plasma-nitrided AISI 316L stainless steel, *Mater. Sci. Eng. A*, 431(2006), No. 1-2, p. 315.
[49] D. Pye, *Practical Nitriding and Ferritic Carburising*, ASM International, Ohio, 2003.
[50] F. Ashrafizadeh, Influence of plasma and gas nitriding on fatigue resistance of plain carbon (Ck45) steel, *Surf. Coat. Technol.*, 174-175(2003), p. 1196.
[51] H. Riazi, F. Ashrafizadeh, S.R. Hosseini, and R. Ghomashchi, Influence of simultaneous aging and plasma nitriding on fatigue performance of 17-4 PH stainless steel, *Mater. Sci. Eng. A*, 703(2017), p. 262.
[52] B. Wu, P.P. Wang, Y.S. Pyoun, J.X. Zhang, and R.I. Murakami, Study on the fatigue properties of plasma nitriding S45C with a pre-ultrasonic nanocrystal surface modification process, *Surf. Coat. Technol.*, 216(2013), p. 191.